NJC

PAPER

Check for updates

The effect of physical morphology and the chemical state of Ru on the catalytic properties of Ru–carbon for cellulose hydrolytic hydrogenation†

Gang Zhang,[ab] Tong Chen, [ID] *[a] Yi Zhang,[ab] Tao Liu[ab] and Gongying Wang[a]

Ru–carbon catalysts with different physical morphologies and chemical states of Ru were prepared by different methods and used to catalyze the hydrolytic hydrogenation of cellulose at high temperatures. The physical morphology of Ru particles and the chemical state of Ru significantly influenced the catalytic performance. The Ru nanoparticles in Ru@MC prepared by the *in situ* carbothermal reduction method exhibited a special chemical state due to the strong interaction with carbon. The special structure could not only prevent the growth of Ru particles but also enhance the hydrogen spillover effect and improve the hydrogenation efficiency. Among the Ru–carbon catalysts, Ru@MC showed the best catalytic performance with a 72.4% yield of sorbitol. Furthermore, the embedded structure of Ru@MC stabilized the Ru nanoparticles, and the catalyst could be reused at least 6 times.

1. Introduction

The conversion of renewable biomass and its derivatives to high-value chemicals and fuels is of significant importance for sustainable social development.[1] Sorbitol, one of the promising platform compounds, has not only been widely used in industrial production such as pharmaceuticals and cosmetics, but also used as a raw material for the preparation of other chemical products such as ethylene glycol and isosorbide.[2,3] Generally, the industrial preparation of sorbitol involves the hydrogenation of glucose, which mainly comes from the hydrolysis of starch.[4] However, starch is mainly derived from edible crops, and its use will compete with the human food supply. Unlike corn and starch, cellulose is one type of renewable inedible biomass and its use will not compete with food supplies. Nevertheless, the primary obstacle for producing sorbitol from cellulose is the high cost of pre-treatment of raw lignocellulose, especially cellulose hydrolysis and purification of glucose from by-products.[5] Therefore, many research studies have been conducted to achieve the direct preparation of sorbitol from cellulose avoiding the degradation of metastable glucose[6] and separation process of intermediate products, thus making sure to obtain high selectivity to high-value chemicals.

The synthesis of sorbitol from cellulose is performed *via* a cascade reaction: hydrolysis of cellulose to glucose *via* acid catalysts and then hydrogenation of glucose into sorbitol over metal catalysts.[7,8] Hot compressed water can dissociate an H$^+$ ion reversibly and promote the hydrolysis of cellulose when the temperature is above 190 °C.[9] A sorbitol yield of 22% was obtained by using commercial ruthenium carbon (Ru/C) in hot compressed water at 245 °C.[10] However, high temperature easily caused polymerization of glucose and hydrogenolysis of sorbitol, thus the yield of sorbitol was low.[11] Subsequent studies have found that the Ru supported on acidic carriers such as sulfonated carbon,[12–14] phosphate,[2] molecular sieve,[15,16] *etc.* could directly promote the conversion of cellulose to sorbitol at low temperatures, reaching a high yield of 71%. However, it should be highlighted that the process was usually time-consuming because the low acidity restrained the hydrolysis rate. The acid–Ru binary catalyst can achieve efficient conversion of cellulose in a short time due to the easy adjustment of the ratio of acidity to reducibility. For example, Geboers *et al.* found that heteropoly acids coupled with Ru/C could effectively improve cellulose conversion, a C6 alcohol (sorbitol + mannitol) yield of 68% was obtained in only 1 h.[17] However, the poor water solubility of heteropoly acids makes them difficult to recycle, which hampered their industrial-scale application. To improve the recoverability and reusability of the solid acid catalyst, Liao *et al.* used zirconium phosphate (ZrP) instead of heteropoly acid as an acid catalyst, and the yield of C6 alcohol reached 85%.[18]

[a] *Chengdu Institute of Organic Chemistry, Chinese Academy of Sciences, Chengdu 610041, Sichuan, P. R. China. E-mail: chentongw@sina.com.cn; Fax: +86 028 85220713; Tel: +86 028 85250005*

[b] *National Engineering Laboratory for VOCs Pollution Control Material & Technology, University of Chinese Academy of Sciences, Beijing 101408, P. R. China*

† Electronic supplementary information (ESI) available. See DOI: 10.1039/d0nj03014g

The Ru–carbon catalyst is crucial for the whole process as it influences the product distribution, promotes cellulose conversion, and reduces the polymerization of hydrolysates. Generally, the Ru physical morphology and chemical state in the catalyst could affect its catalytic performance and stability. For example, modifying carbon materials with hydrophilic groups[19] or introducing a dopant (N, P) into carbon materials[6] could decrease the metal-nanoparticle size and improve the catalytic activity. However, the conventional supported Ru catalysts exhibit a weak interaction between Ru and the support to immobilize them, so Ru catalysts easily deactivate under hydrothermal conditions, due to the leaching, sintering, and partial oxidation of Ru nanoparticles.[20] We recently found that the combination of Ru/MC and ZrP was effective in the conversion of cellulose to sorbitol.[21] However, the Ru/MC deactivated severely, and the yield of sorbitol was only 30.9% for the fourth use. Therefore, it is necessary to develop a new preparation strategy, which would improve the stability of Ru nanoparticles. Several attempts have been made to provide Ru with more stability, such as intensifying the bonding between the support and metal,[22] or encapsulating metal particles in a support,[23] but this is not sufficient under harsh reaction conditions. Recently, metals embedded in supports have received much attention as a methodology to obtain stable catalysts.[24–26] Researchers found that Ru semi-embedded in the support could facilitate the strong metal–support interaction (SMSI) between Ru and the support to inhibit agglomeration and leaching of Ru nanoparticles, and exhibited excellent stability in the reaction of ammonia synthesis,[27] hydrogenation of levulinic acid[24] and benzoic acid.[28] Besides, the existence of SMSI between Ru and carbon could also change the chemical state of Ru and improve the hydrogenation activity.[29] While such research has not been carried out for the direct synthesis of sorbitol from cellulose.

In this study, the use of Ru embedded in a carbon catalyst was intended to increase the stability of the catalyst, but we unexpectedly found that it also improved the hydrogenation activity of the catalyst in the hydrolytic hydrogenation of cellulose. Therefore, to investigate the influence of the physical morphology of Ru and chemical state of Ru@MC on the hydrolytic hydrogenation of cellulose, Ru carbon catalysts with different structures were prepared by the *in situ* carbothermal reduction method and the impregnation method. The results showed that the embedded structure of Ru@MC significantly changed the physical morphology and chemical state of Ru, enhancing the interaction between Ru and carbon. Ru@MC exhibited terrific catalytic activity and reliable reusability in the hydrolytic hydrogenation of cellulose in hot compressed water.

2. Experimental

2.1 Catalyst preparation

Ruthenium supported on carbon (Ru/MC). 5.0 g SiO_2, 10.5 g sucrose, and 1.5 g citric acid were ground together for 1 hour. The mixture was placed in an oven at 100 °C for 6 h and heated to 160 °C, and kept for another 6 h. Then, the yellow powder

was heated to 750 °C and kept for 3 h with the protection of N_2. Finally, the obtained black powder was washed with hot sodium hydroxide solution to remove silica. The obtained black powder was denoted as MC. Ru/MC was prepared by the wet impregnation method. The obtained MC was used as the support and added to the 15 mL aqueous solution containing 0.07 g $RuCl_3$. Then the samples were dried at 120 °C overnight. The sample was reduced at 300 °C for 2 h under a H_2 flow before use, and denoted as Ru/MC.

Ruthenium embedded in mesoporous carbon (Ru@MC). The Ru@MC was prepared according to the literature[30] with a little modification. 5.0 g SiO_2 was added into 10 mL of an aqueous solution containing 0.07 g of $RuCl_3·3H_2O$, and allowed to stand for 12 h. Then the mixture was dried at 110 °C for 12 h to obtain $RuCl_3/SiO_2$. $RuCl_3/SiO_2$ was used as a hard template and ground with sucrose and citric acid for 1 h. The mixture was then placed in an oven at 100 °C for 6 h and heated to 160 °C, and kept for another 6 h to obtain the catalyst precursor ($Ru/SiO_2@C$). Then, the precursor was heated to 750 °C and kept for 3 h with the protection of N_2. Finally, the black powder was washed with hot sodium hydroxide solution to remove silica. The obtained black powder was denoted as Ru@MC. Note that oxidized Ru was reduced during carbonization, thus, the reduction of catalysts with hydrogen or other reductants was unnecessary. The obtained catalyst was calcined at 450 °C and 550 °C under a N_2 atmosphere, and denoted as Ru@MC$_{-450}$ and Ru@MC$_{-550}$.

Coated ruthenium carbon (Ru@C). $RuCl_3$, sucrose, and citric acid were ground together for 1 h. The mixture was then placed in an oven at 100 °C for 6 h and heated to 160 °C, and kept for another 6 h. Then, the black powder was heated to 750 °C and kept for 3 h with the protection of N_2, the obtained black powder was denoted as Ru@C.

Ruthenium reference. Commercial ruthenium carbon (Ru/C, Aladdin, 5 wt% Ru) was used as a reference sample.

2.2 Catalyst characterization

Thermogravimetric analysis (TGA) was conducted on a TA Q50 TG instrument, the sample was heated from 30 °C to 900 °C with a temperature ramp rate of 10 °C min^{-1} under a N_2 flow. The nitrogen sorption isotherms of the catalyst were determined by a Micromeritics ASAP 2020 apparatus with N_2 (at −196 °C) as the sorbate. XRD patterns were obtained on a Thermo ESCALAB 250XI diffractometer using Cu Kα (1.54 Å) with 2θ between 10° and 80° with a step size of 0.02°. CO chemisorption was conducted on an AutoChem1 II 2920 chemisorption instrument. First of all, the samples were loaded into a quartz tube, and heated to 300 °C for 2 h in H_2. Then cooled to room temperature and flushed with nitrogen for 1 h. Finally, the static adsorption of the CO molecule was performed at 40 °C. H_2-TPD was also performed on an AutoChem1 II 2920 chemisorption instrument. Before measuring, the sample was heated to 150 °C and kept for 30 min under a He atmosphere, and cooled to room temperature. The sample was reduced in a 10% H_2/N_2 flow at 300 °C. Then the sample was cooled to room temperature and exposed to H_2 for 30 min. After being flushed with He for 2 h, the

temperature-programmed desorption was performed in a He stream at a flow rate of 30 mL min^{-1} with a temperature ramp rate of 10 °C min^{-1}. Transmission electron microscopy (TEM) and high-resolution TEM (HRTEM) micrographs were recorded on a JEOL 2100F instrument. X-ray photoelectron spectroscopy (XPS) was recorded on an ESCALAB 250 X-ray photoelectron spectrometer equipped with a monochromated micro-focused Al X-ray source.

2.3 Catalyst evaluation

The testing experiments of the catalytic activity of the catalysts for glucose hydrogenation or cellulose conversion was performed in a 100 mL stainless steel autoclave reactor agitated with a magnetic stirring bar. 50 mL of glucose aqueous solution (0.1 mol L^{-1}) or 0.5 g of cellulose and a certain amount of catalyst were loaded in the reactor. Then, the reactor was flushed with N$_2$ to evacuate air and charged with H$_2$. When the test finished, the reactor was quickly placed into an ice bath. The liquid products were separated by filtration. Qualitative and quantitative analysis of liquid products were conducted on a high-performance liquid chromatography (Waters e2695) system. The solid was collected after reaction by filtration and washed with water and ethanol. The catalyst was then dried for 2 h at 65 °C in a vacuum oven. Finally, the obtained catalyst was reused to conduct new tests under the aforementioned reaction conditions.

3 Results and discussion

3.1 Catalyst characterization

The porosity of the samples was determined by N$_2$ absorption–desorption characterization. The isotherms and pore size distribution of four samples prepared by different methods are shown in Fig. 1. Ru@MC and Ru/MC exhibited typical type-IV isotherms with an H2 hysteresis loop, which was a typical characteristic of mesoporous materials.[31] The shape of the hysteresis loop indicated the existence of large uniform mesopores,[32] and the pore size was centered at 10 nm. The isotherm of Ru/C was type-IV with an H4 hysteresis loop. The amount of adsorbed N$_2$

was rapidly increased under the low P/P_0 (<0.2), and the pore size distribution was centered at <2 nm and 3.5 nm, suggesting that Ru/C was a hierarchically structured porous material with micropores and mesopores. The isotherm of Ru@C was type-II without hysteresis loops, indicating the absence of the porous structure. The BET surface area, average pore diameter, and mesopore surface area of the samples are listed in Table 2. The specific areas of Ru@MC and Ru/MC were 866 m^2 g^{-1} and 858 m^2 g^{-1}, and the mesopore surface areas reached 689 m^2 g^{-1} and 667 m^2 g^{-1}, respectively, meaning that the Ru@MC and Ru/MC mainly had a mesoporous structure. However, the specific area of Ru@C was very small, and mainly the external surface. Besides, even though the specific surface area of Ru/C was up to 1027 m^2 g^{-1}, the mesopore surface area was only 485 m^2 g^{-1}, indicating that the dominant pore structure was micropores. The physical structure of the catalysts had an important effect on their catalytic performance. Ru@MC and Ru/MC, prepared with the hard template, both exhibited high specific surface areas and large pore sizes, which would facilitate the large molecule transport (Table 1).

The XRD patterns of the samples are given in Fig. 2. The existence of two weak and broad diffraction peaks at around 20° and 45° revealed that all samples have an amorphous carbon structure.[33] The XRD patterns of Ru@MC and MC were similar, indicating that the introduction of Ru species didn't change the structure of MC. For Ru@MC and Ru/MC, the absence of Ru diffraction peaks indicated the Ru nanoparticles were highly dispersed in the two samples. It should be noted that no signal of Ru was detected after the thermal treatment of Ru@MC at 450 °C, indicating the high stability of Ru@MC. Sucrose directly interacted with cationic Ru during the preparation of Ru@MC, so the abundant hydroxyl groups of sucrose could stabilize the cationic Ru.[30] Nevertheless, a weak peak was observed at 44° for Ru/MC-450, illustrating that the Ru nanoparticles were easy to sinter at high temperatures due to the weak interaction between Ru and the carbon support. Ru@C was prepared by direct carbonization of the RuCl$_3$–sucrose mixture without SiO$_2$ and the XRD result showed no peak of Ru, further confirming that abundant hydroxyl groups could stabilize Ru, inhibiting the sintering of Ru particles during the carbonization. The above result suggested that preparation methods had important influence on the dispersion and stability of Ru catalysts. Ru@MC prepared by an *in situ* carbothermal reduction method not only made Ru highly dispersed, but also stabilized the Ru nanoparticles. While the Ru nanoparticles in Ru/MC were easy to sinter at high temperatures.

The TEM images of Ru catalysts prepared by different methods and Ru@MC-450 are shown in Fig. 3. The average particle sizes of Ru@MC (Fig. 3(a)) and Ru@MC-450 (Fig. 3(c))
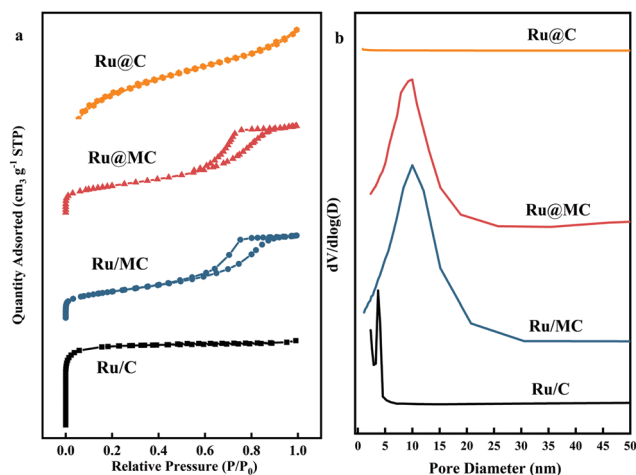

Fig. 1 N$_2$ sorption isotherms and pore size distribution of four samples.

Table 1 Pore features of the Ru catalysts

Samples	S_{BET} (m^2 g^{-1})	S_{meso} (m^2 g^{-1})	D (nm)
Ru@MC	866	689	6.5
Ru/MC	858	667	6.8
Ru@C	20	—	—
Ru/C	1027	485	1.8
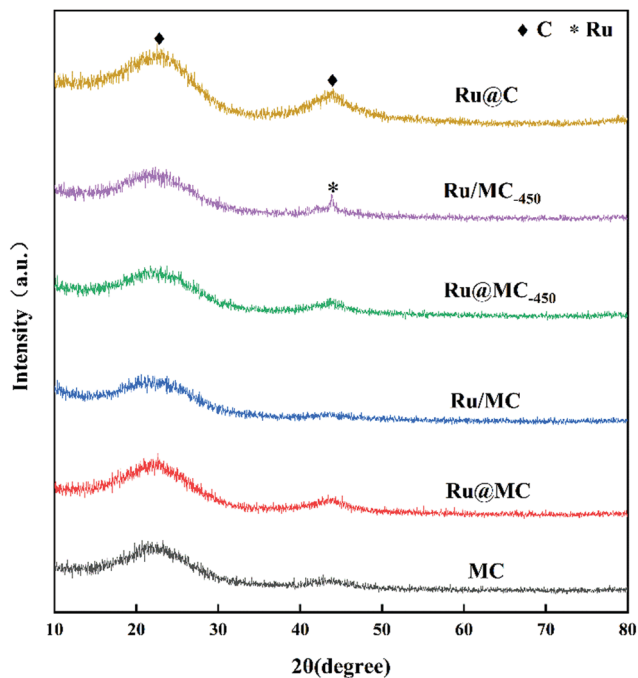
Fig. 2 XRD patterns of various Ru carbon catalysts and MC.

Fig. 3 TEM images of Ru–carbon catalysts. (a and b) Ru@MC, (c) Ru@MC$_{-450}$, (d) Ru@C, and (e) Ru/MC, (inset in (a), (c), (d), and (e) are the particle size distribution estimated by TEM).

were 3.5 nm and 3.3 nm, respectively, indicating that Ru nanoparticles were homogeneously dispersed on the MC and exhibited high stability. As shown in the HRTEM image (Fig. 3(b)), the characteristic spacing of 0.20 nm agreed well with the Ru (101) crystallographic planes (PDF number 89-4903), indicating that the oxidized Ru was reduced to metallic Ru^0 during the carbonization. The TEM image of Ru@C is shown in Fig. 3(d). The average particle size of Ru@C was 2.8 nm, which was smaller than that of Ru@MC, because sucrose stabilized Ru more efficiently without the presence of the template.[30] This result was identical to the results of XRD. The TEM image of Ru/MC is given in Fig. 3(f). The average particle size was 2.6 nm, and the existence of large particles indicated that Ru nanoparticles were heterogeneously dispersed on the support.

The dispersion of Ru in the samples was conducted by CO chemisorption, and the results are listed in Table 2. The amount of CO chemisorbed on Ru@C, Ru/C Ru@MC, and Ru/MC is 12.5 µmol g^{-1} cat, 45.7 µmol g^{-1} cat, 25.0 µmol g^{-1} cat and 59.8 µmol g^{-1} cat, respectively. The dispersion of Ru in Ru@C was the lowest among the four catalysts, as Ru nanoparticles were completely coated with carbon, the CO molecules could not come into contact with the Ru nanoparticles. It should be noted that even though Ru/C exhibited a high specific surface area, the dispersion of Ru was only 45.7%, which was lower than that of Ru/MC. The reason was that the Ru loading of Ru/C was 4.96%, while the Ru loading of Ru/MC was only 1.09%. According to the nitrogen absorption–desorption and ICP-OES, the specific area and the Ru loading were almost the same, but the dispersion Ru in Ru@MC was much smaller than that in Ru/MC. Besides, according to the particle size of Ru calculated from CO chemisorption and TEM analysis, Ru particle sizes measured by two methods were almost the same, while
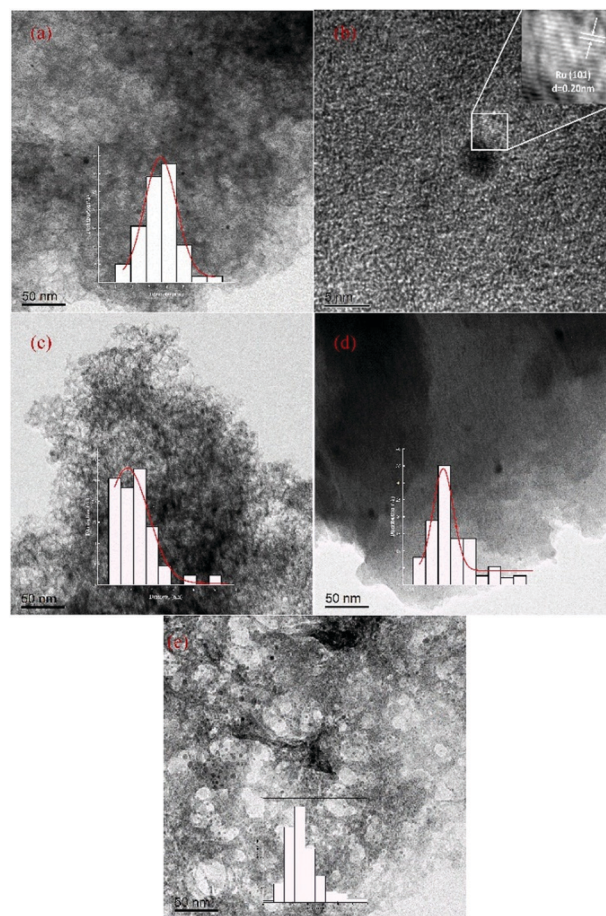
Table 2 Ru dispersion in Ru@MC, Ru/MC, Ru/C, and Ru@C determined by CO chemisorption

Samples	Ru loading	CO uptake (µmol g^{-1} cat)	Dispersion (%)	Particle size (nm)	
				By CO chemisorption	By TEM
Ru@MC	0.97	25.0	26.1	5.2	3.5
Ru/MC	1.09	59.8	55.4	2.4	2.6
Ru/C	4.96	224.3	45.7	2.9	—
Ru@C	0.94	12.5	13.4	9.9	2.8

Ru particle sizes of Ru@MC and Ru@C calculated by CO chemisorption were much larger than that determined by TEM analysis. This was because in Ru@MC and Ru@C, Ru particles were coated with carbon, which would inhibit the contact of the CO molecule with Ru. Therefore, the dispersion and particle size were overestimated.[28] According to a previous study,[31] the embedding degree of the catalyst was obtained from the formula $D_{embedding} = (1 - N_s/N_c) \times 100\%$, where N_s and N_c refer to the number of metal atoms on the surface and the average crystallite size, respectively. The $D_{embedding}$ of Ru@MC was 32.7%, indicating that the *in situ* carbothermal reduction method could successfully semi-embed Ru nanoparticles in the

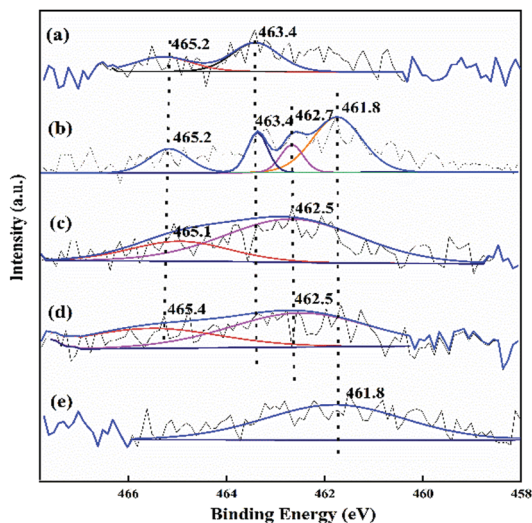Fig. 4 XPS spectra of Ru 3p core levels of (a) Ru/SiO$_2$@C, Ru@MC carbonized at 550 °C (b) and 750 °C (c), Ru@MC calcined at 450 °C (d), and Ru/MC (e).

Fig. 5 The H$_2$-TPD profile of Ru@MC.

carbon matrix. The CO chemisorption results suggested that different preparation methods could affect the physical morphology of the exposed Ru active site of catalysts. The Ru particles of Ru@MC were semi-embedded in the MC. Ru nanoparticles of the three catalysts were either semi-embedded in the carbon, or supported on the surface of carbon, or completely coated with carbon.

XPS was performed to obtain information on the chemical state Ru in the samples, the analytical results are shown in Fig. 4. Before carbonization, the Ru 3p$_{3/2}$ binding energy (BE) of the Ru/SiO$_2$@C was deconvoluted into two peaks, which correspond to Ru^{4+} (463.4 eV) and Ru^{6+} (465.2 eV), indicating the oxidized Ru was the major component. After being carbonized at 550 °C, the BE of Ru 3p$_{3/2}$ was deconvoluted into four peaks. The peak at *ca.* 461.8 eV was attributed to Ru^0,[34] revealing that oxidized Ru was reduced to Ru^0 during the carbonization. The peaks at *ca.* 463.4 eV and 465.2 eV were attributed to the oxidized Ru, indicating that the Ru could not be fully reduced at 550 °C. Note that a new peak at around 462.7 eV, between metallic and oxidized Ru, was observed, which is possibly because the p orbital of carbon formed a hybrid orbital with the d orbital of Ru during the carbonization process and the BE of Ru exhibited a positive shift.[35] Upon being carbonized at 750 °C, the dominant peak appeared at around 462.5 eV and the peak at ∼461.8 eV disappeared, demonstrating that the oxidized Ru was almost fully reduced and SMSI existed between Ru and carbon, which further influenced the BE of Ru^0. Therefore, it is obvious that the *in situ* carbothermal reduction method could affect the chemical state of Ru. The XPS pattern of Ru@MC$_{-450}$ was similar to that of Ru@MC, illustrating that the chemical state of Ru didn't changed after being calcined at high temperature under a N$_2$ flow. For Ru/MC, the peak at 461.8 eV was ascribed to Ru^0, indicating that Ru^{3+} was completely reduced.

The H$_2$-TPD profile of Ru@MC is shown in Fig. 5. The peak at around 200 °C was ascribed to the stoichiometric chemisorption of h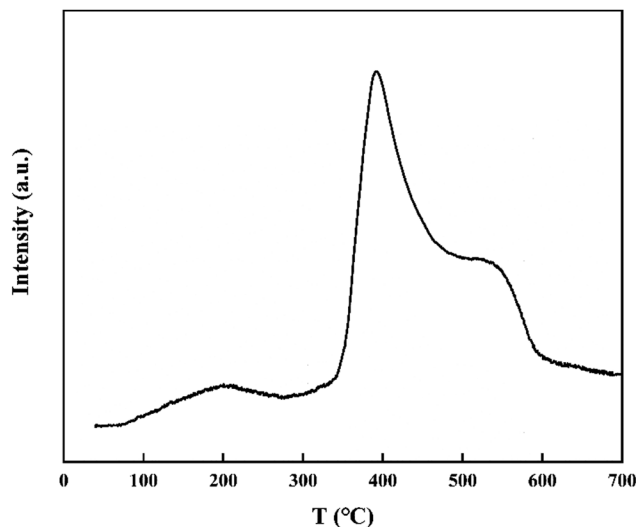ydrogen on Ru sites[36] and the dispersion of Ru was 30.1%, which was similar to that based on CO chemisorption. The H$_2$ desorption peak at 400 °C was ascribed to the Ru sites covered by spillover hydrogen, illustrating that the SMSI between Ru and carbon promoted the hydrogen spillover effect.[37]

3.2 Glucose hydrogenation

To study the effect of physical morphology, chemical state, and pore size of Ru–carbon catalysts on the glucose hydrogenation, glucose hydrogenation was performed separately, and the results are presented in Table 3. The hydrogenation performance of the three catalysts prepared by different methods was quite different. Ru@MC showed the best catalytic activity, and the sorbitol yield was 99.3%. Ru@C gave the lowest sorbitol yield. Although the Ru nanoparticles in Ru@C were homogeneously and highly dispersed on carbon, most of Ru nanoparticles were completely coated with carbon, and they could not be exposed to reactants during the reaction. Ru loading and pore structure of Ru@MC and Ru/MC were almost the same, but Ru@MC exhibited better hydrogenation activity than Ru/MC, which was ascribed to the special chemical state of Ru promoting the transport of adsorbed and dissociated hydrogen from Ru to the support for hydrogen spillover and hydrogenation reactions.[38] Thus, the TOF of Ru@MC was up to 1128 h^{-1}, which was almost two times higher than that of Ru/MC. Furthermore, the hydrogenation activity of Ru/C was as good as that of Ru@MC, but the selectivity to sorbitol was inferior to that of Ru@MC. This was because the microporous structure of Ru/C could easily cause side reactions. The results of glucose hydrogenation demonstrated that the excellent hydrogenation performance of Ru@MC was ascribed to its special structure, which enhanced the hydrogenation efficiency. Besides, when the catalyst was calcined at 450 °C and 550 °C under a N$_2$ flow for 2 h, the catalytic activity did not significantly decline, indicating that the Ru@MC had high thermal stability.

Compared with previous works,[12,15,39,40] Ru@MC enhanced the hydrogenation efficiency and exhibited excellent hydrogenation

Table 3　Catalytic performance of various catalysts for the conversion of glucose to sorbitol

| Catalysts | Ru loading/wt% | t/h | P/MPa | Conv./% | Yield/% | | TOF/h^{-1} | Ref. |
					Sorbitol	Mannitol		
Ru@MC	0.97	2	2	100	99.3	0.2	1128	This work
Ru/MC	1.09	2	2	89.2	88.4	0.6	503	This work
Ru/C	4.97	2	2	100	86.3	12.6	210	This work
Ru@C	0.94	2	2	22.8	22.2	—	480	This work
Ru@MC-450	—	2	2	100	99.1	0.8	—	This work
Ru@MC-550	—	2	2	100	99.0	0.8	—	This work
Ru/CCD	5	1.5	3	99.7	98.6	1.0	—	12
Ru/MCM-41	5	1.5	3	100	83.1	—	—	15
Ru/NiO_TiO$_2$	1	2	5.5	94.9	92.2	—	—	39
Ru/HYZ	1	2	5.5	100	98.7	0.7	—	40

Reaction temperature: 120 °C.

activity, thus a high yield of sorbitol could be obtained with the complete conversion of glucose under the relatively low H$_2$ pressure.

The effect of the carbonization temperature of Ru@MC catalytic activity on glucose hydrogenation was investigated, and the results are shown in Fig. S2 (ESI†). It was obvious that the carbonization temperature significantly influenced the hydrogenation of glucose. When the carbonization temperature was 550 °C, the glucose conversion and sorbitol yield were only 26.1% and 23.0%, respectively. With the increase in the carbonization temperature, the glucose conversion and sorbitol yield were escalated significantly. The yield of sorbitol was up to 99.3% with the complete conversion of glucose when the carbonization temperature was 750 °C. Upon further increasing the carbonization temperature, the glucose conversion and sorbitol yield remained constant. The above-mentioned results revealed that under low carbonization temperature, the catalytic activity of Ru@MC was poor because Ru^{3+} was partially reduced, which was confirmed by the XPS result. When carbonization temperature was higher than 750 °C, most of Ru^{3+} was reduced to Ru^0 and exhibited outstanding hydrogenation activity. Therefore, the optimal carbonization temperature was 750 °C.

3.3 Hydrolytic hydrogenation of cellulose

In the synthesis of sorbitol from cellulose, the hydrogenolysis of sorbitol would be dominated and the yield of sorbitol reduced if the hydrolysis rate of cellulose was too slow.[19] Thus, to promote the hydrolysis rate, ZrP was chosen as the acid catalyst

for cellulose hydrolysis due to its abundant acid sites, water tolerance, easy preparation, and good hydrothermal stability.[41] The performance of Ru@MC combined with ZrP in hydrolytic hydrogenation of cellulose was determined, and the results are given in Table 4. The hydrolytic hydrogenation of cellulose was performed at 170 °C with an H$_2$ pressure of 5.0 MPa. For Ru/MC, a yield of 46.4% was obtained with a 90.6% conversion of cellulose. Although the Ru/C gave 100% conversion of cellulose, the yield of sorbitol was only 40.1%. Ru@MC gave the highest sorbitol yield with the complete conversion of cellulose, indicating the high hydrogenation efficiency could improve the cellulose conversion and sorbitol yield simultaneously. As reported in previous works,[42,43] if the catalyst and cellulose were pretreated by mix-milling, both the crystallinity and the polymerization degree of cellulose were decreased, facilitating the hydrolysis of cellulose.[7] Hence, when cellulose and ZrP were mix-milled together, the cellulose conversion and sorbitol yield reached 100% and 72.4% at 170 °C in just 1.5 h, respectively.

The results of previous studies are also listed in Table 4.[2,10,14,17,18] To date, a high yield of 71.1% was obtained with the Ru/AC–SO$_3$H catalyst, but the process was time-consuming. The combination of Ru/C with the acid catalyst was effective in the conversion of cellulose, while the selectivity to sorbitol was poor and the products were usually the mixture of sorbitol and mannitol. In this work, Ru@MC exhibited high selectivity to sorbitol, thus a high sorbitol yield was obtained at low temperatures with a short reaction time.

Table 4　Catalytic performance of various catalysts for the conversion of cellulose to sorbitol

| Catalysts | Ru loading/wt% | T/°C | P/MPa | t/h | Conv./% | Yield/% | | Ref. |
						Sorbitol	Mannitol	
Ru/MC	1.09	170	5	3.5	90.6	46.4	2.4	This work
Ru/C	4.97	170	5	3.5	100	40.1	13.1	This work
Ru@MC	0.97	170	5	3.5	100	61.5	3.6	This work
Ru@MC^a	0.97	170	5	1.5	100	72.4	2.5	This work
Ru/NbOPO$_4$	5	170	4	24	100	69.1	1.3	2
Ru/C	5	245	6	0.5	85.5	22.2	9.7	10
Ru/AC-SO$_3$H	10	165	5	36	100	71.1	—	14
Ru/C^b	5	180	5	2	99	68^c		17
Ru/C^d	5	190	6	2.5	94.7	85.5^c		18

^{a} Cellulose and ZrP were mix-milled. ^{b} H$_4$SiW$_{12}$O$_{40}$ were used as the acid catalyst. ^{c} C6 (sorbitol and mannitol) yield. ^{d} ZrP were used as the acid catalyst.
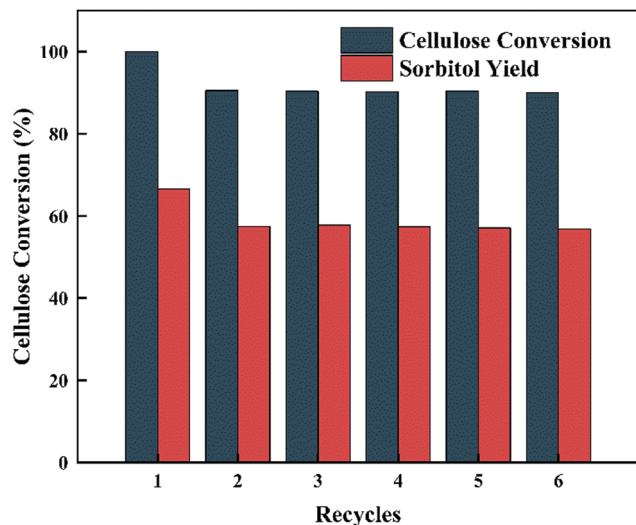
Fig. 6 The recyclability of Ru@MC for cellulose conversion. Reaction conditions: Cellulose 0.5 g, ZrP 0.9 g, Ru@MC 60 mg, H_2O 50 mL, 5 MPa H_2, 170 °C, 3.5 h.

3.4 Recyclability of the catalyst

The recycling experiments of Ru@MC combined with ZrP for the hydrolytic hydrogenation of cellulose were performed under the optimized reaction conditions and the results are shown in Fig. 6. The cellulose conversion and sorbitol yield declined to 90.6% and 52.5% in the second run, respectively. The P leaching of fresh ZrP under the hydrothermal reaction conditions was responsible for the decreased sorbitol yield, which has been confirmed in the previous studies.[18] Then, the catalysts of Ru@MC combined with ZrP remained catalytic activity in the subsequent operations and could be used at least 6 times.

To further confirm the stability of Ru@MC, the recycling experiments of Ru@MC in glucose hydrogenation without ZrP were also performed and the results are shown in Fig. 7.
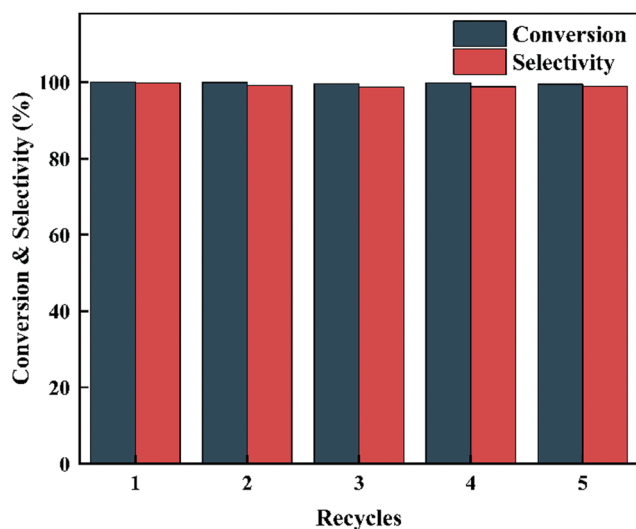

Fig. 7 The recyclability of Ru@MC for glucose hydrogenation. Reaction conditions: glucose 50 g (0.1 mol L^{-1}), Ru@MC 80 mg, 120 °C, 2 MPa H_2, 2 h.

Ru@MC exhibited excellent stability and there was no obvious loss of activity even after being reused 5 times, and the selectivity of sorbitol remained above 99% each time, indicating that the embedded structure could enhance the stability of the catalyst.

4. Conclusion

In this study, Ru–carbon catalysts with different structures were prepared to investigate the effect of the physical morphology and chemical state of Ru on the conversion of cellulose. Ru embedded in the mesoporous carbon catalyst was used for the first time in the synthesis of sorbitol from cellulose. Compared with the traditional Ru supported catalysts, the Ru@MC catalyst changed the physic morphology and chemical state of Ru simultaneously and intensified the interaction between Ru and carbon, improving the hydrogen spillover effect and hydrogenation efficiency. Hence, the TOF of Ru@MC on the glucose hydrogenation was much higher than that of Ru/MC. Ru@MC exhibited outstanding activity and stability in the synthesis of sorbitol from cellulose. The yield of sorbitol was over 70% in just 1.5 h of reaction. Furthermore, Ru@MC could be reused at least 6 times.

Conflicts of interest

There are no conflicts to declare.

Acknowledgements

References

1 S. Van de Vyver, J. Geboers, P. A. Jacobs and B. F. Sels, *ChemCatChem*, 2011, **3**, 82–94.

2 J. Xi, Y. Zhang, Q. Xia, X. Liu, J. Ren, G. Lu and Y. Wang, *Appl. Catal., A*, 2013, **459**, 52–58.

3 M. Dolores Adsuar-Garcia, J. Xavier Flores-Lasluisa, F. Zahra Azar and M. Carmen Roman-Martinez, *Catalysts*, 2018, 8.

4 S. Esposito, B. Silvestri, V. Russo, B. Bonelli, M. Manzoli, F. A. Deorsola, A. Vergara, A. Aronne and M. Di Serio, *ACS Catal.*, 2019, **9**, 3426–3436.

5 N. Rey-Raap, L. S. Ribeiro, J. J. de Melo Orfao, J. L. Figueiredo and M. F. Ribeiro Pereira, *Appl. Catal., B*, 2019, 256.

6 X. Zhao, J. Xu, A. Wang and T. Zhang, *Chin. J. Catal.*, 2015, **36**, 1419–1427.

7 L. S. Ribeiro, J. J. Delgado, J. J. M. Orfao and M. F. R. Pereira, *Appl. Catal., B*, 2017, **217**, 265–274.

8 W. Deng, X. Tan, W. Fang, Q. Zhang and Y. Wang, *Catal. Lett.*, 2009, **133**, 167–174.

9 H. Kobayashi, Y. Ito, T. Komanoya, Y. Hosaka, P. L. Dhepe, K. Kasai, K. Hara and A. Fukuoka, *Green Chem.*, 2011, **13**, 326–333.

10 C. Luo, S. Wang and H. Liu, *Angew. Chem., Int. Ed.*, 2007, **46**, 7636–7639.

11 G. Liang, L. He, H. Cheng, W. Li, X. Li, C. Zhang, Y. Yu and F. Zhao, *J. Catal.*, 2014, **309**, 468–476.

12 Z. Li, Y. Liu and S. Wu, *BioResources*, 2018, **13**, 1278–1288.

13 A. Onda, T. Ochi and K. Yanagisawa, *Top. Catal.*, 2009, **52**, 801–807.

14 J. W. Han and H. Lee, *Catal. Commun.*, 2012, **19**, 115–118.

15 J. Zhang, L. Lin, J. Zhang and J. Shi, *Carbohydr. Res.*, 2011, **346**, 1327–1332.

16 A. Romero, A. Nieto-Marquez and E. Alonso, *Appl. Catal., A*, 2017, **529**, 49–59.

17 J. Geboers, S. Van de Vyver, K. Carpentier, K. de Blochouse, P. Jacobs and B. Sels, *Chem. Commun.*, 2010, **46**, 3577–3579.

18 Y. Liao, Q. Liu, T. Wang, J. Long, L. Ma and Q. Zhang, *Green Chem.*, 2014, **16**, 3305–3312.

19 B. F. Machado, M. Oubenali, M. Rosa Axet, T. Trang Nguyen, M. Tunckol, M. Girleanu, O. Ersen, I. C. Gerber and P. Serp, *J. Catal.*, 2014, **309**, 185–198.

20 Y. Zhang, M. Zhao, H. Wang, H. Hu, R. Liu, Z. Huang, C. Chen, D. Chen and Z. Feng, *Bioresour. Technol.*, 2019, **288**, 121532.

21 G. Zhang, T. Chen, Y. Zhang, T. Liu and G. Wang, *Catal. Lett.*, 2020, **150**(8), 2294–2303.

22 J. Ftouni, A. Munoz-Murillo, A. Goryachev, J. P. Hofmann, E. J. M. Hensen, L. Lu, C. J. Kiely, P. C. A. Bruijnincx and B. M. Weckhuysen, *ACS Catal.*, 2016, **6**, 5462–5472.

23 Z. Wei, Y. Chen, J. Wang, D. Su, M. Tang, S. Mao and Y. Wang, *ACS Catal.*, 2016, **6**, 5816–5822.

24 Z. Wei, J. Lou, C. Su, D. Guo, Y. Liu and S. Deng, *ChemSusChem*, 2017, **10**, 1720–1732.

25 H. Wang, C. Chen, H. Zhang, G. Wang and H. Zhao, *Chin. J. Catal.*, 2018, **39**, 1599–1607.

26 F. Su, L. Lv, F. Y. Lee, T. Liu, A. I. Cooper and X. S. Zhao, *J. Am. Chem. Soc.*, 2007, **129**, 14213–14223.

27 Y. Zhou, Y. Ma, G. Lan, H. Tang, W. Han, H. Liu and Y. Li, *Chin. J. Catal.*, 2019, **40**, 114–123.

28 Z. Jiang, G. Lan, X. Liu, H. Tang and Y. Li, *Catal. Sci. Technol.*, 2016, **6**, 7259–7266.

29 X. Liu, G. Lan, P. Su, L. Qian, T. Ramirez Reina, L. Wang, Y. Li and J. Liu, *Catal. Today*, 2020, **351**, 75–82.

30 Y. Li, G. Lan, H. Wang, H. Tang, X. Yan and H. Liu, *Catal. Commun.*, 2012, **20**, 29–35.

31 Y. Zhang, T. Chen, G. Zhang, G. Wang and H. Zhang, *Appl. Catal., A*, 2019, **575**, 38–47.

32 S. K. Das, M. K. Bhunia, A. K. Sinha and A. Bhaumik, *ACS Catal.*, 2011, **1**, 493–501.

33 K. Nakajima and M. Hara, *ACS Catal.*, 2012, **2**, 1296–1304.

34 M. Guo, G. Lan, J. Peng, M. Li, Q. Yang and C. Li, *J. Mater. Chem. A*, 2016, **4**, 10956–10963.

35 Y.-X. Xiao, J. Ying, G. Tian, Y. Tao, H. Wei, S.-Y. Fan, Z.-H. Sun, W.-J. Zou, J. Hu, G.-G. Chang, W. Li, X.-Y. Yang and C. Janiak, *Appl. Catal., B*, 2019, **259**.

36 B. Zhang, Q. Wu, C. Zhang, X. Su, R. Shi, W. Lin, Y. Li and F. Zhao, *ChemCatChem*, 2017, **9**, 3646–3654.

37 R. Prins, *Chem. Rev.*, 2012, **112**, 2714–2738.

38 S. D. Lin and M. A. Vannice, *J. Catal.*, 1993, **143**, 539–553.

39 D. K. Mishra, J.-M. Lee, J.-S. Chang and J.-S. Hwang, *Catal. Today*, 2012, **185**, 104–108.

40 D. K. Mishra, A. A. Dabbawala, J. J. Park, S. H. Jhung and J.-S. Hwang, *Catal. Today*, 2014, **232**, 99–107.

41 G. Gliozzi, A. Innorta, A. Mancini, R. Bortolo, C. Perego, M. Ricci and F. Cavani, *Appl. Catal., B*, 2014, **145**, 24–33.

42 H. Kobayashi, M. Yabushita, T. Komanoya, K. Hara, I. Fujita and A. Fukuoka, *ACS Catal.*, 2013, **3**, 581–587.

43 M. Yabushita, H. Kobayashi, K. Hara and A. Fukuoka, *Catal. Sci. Technol.*, 2014, **4**, 2312–2317.